Phase Plane Analysis of Quantized Congestion Notification for Data Center Ethernet

Wanchun Jiang, Fengyuan Ren, *Member, IEEE*, and Chuang Lin, *Senior Member, IEEE*

***Abstract*—Currently, Ethernet is being enhanced to become the unified switch fabric in data centers. With the unified switch fabric, the cost on redundant devices is reduced, while the design and management of data center networks are simplified. Congestion management is one of the indispensable enhancements on Ethernet, and Quantized Congestion Notification (QCN) has just been ratified as the formal standard. Though QCN has been investigated for several years, there exist few in-depth theoretical analyses on QCN. The most possible reason is that QCN is heuristically designed and involves the property of variable structure. The classic linear analysis method is incapable of handling the segmented nonlinearity of the variable structure system. In this paper, we use the phase plane method, which is suitable for systems of segmented nonlinearity, to analyze the QCN system. The overall dynamic behaviors of the QCN system are presented, and the sufficient conditions for the stable QCN system are deduced. These sufficient conditions serve as guidelines toward proper parameters setting. Moreover, we find that the stability of QCN is mainly promised by the sliding mode motion, which is the underlying reason for QCN's stable queue shown in numerous simulations and experiments. Experiments on the NetFPGA platform verify that the analytical results can explain the complex behaviors of QCN.**

***Index Terms*—Phase plane analysis, quantized congestion notification, sliding mode motion, stability.**

I. Introduction

THROUGH network, data centers integrate tens of thousands of computers into a powerful computing infrastructure, benefiting from the economies of scale. In today's data centers, it is common to deploy an Ethernet network for IP traffic, one or two storage area networks (SANs) for block-mode Fibre Channel traffic, and an InfiniBand network for High Performance Computing (HPC) traffic. Each of them has its own characters. Ethernet is feature-rich, simple, cheap, and broadly used, SANs require no packets loss, while InfiniBand desires extremely low latency. This hybrid network not only dramatically increases the cost on cables, switches, and transceivers, but also complicates the design, operation, and management of data center networks (DCNs). As the size of data centers grows, problems are getting worse. The unified switch fabric is being developed to solve these problems [1], [6], [24].

With the recent advances in the speed of 10 Gb/s and the ratification of the standard for 40 Gb/s and 100 Gb/s [7], Ethernet is chosen to be enhanced as the unified switch fabric in data centers by the IEEE 802.1 Data Center Bridging (DCB) work group [1]. The enhanced Ethernet is called Data Center Ethernet (DCE) or Converged Enhanced Ethernet (CEE). Meanwhile, Fiber Channel over Ethernet (FCoE) is developed to accommodate storage traffic on lossless Ethernet [20], and techniques such as MXoE [22] and RoCEE [19] are investigated to carry HPC traffic over Ethernet of low latency. On the other hand, DCE begins to appear in industry platforms, such as the Unified Computing System of Cisco [5].

As a best-effort network technique, Ethernet needs further enhancements to satisfy additional requirements of DCNs, such as extremely low latency and no packets loss. Accordingly, several enhancement mechanisms of Ethernet are standardized within the IEEE 802.1 DCB work group. Priority-based flow control mechanism is one of these enhancement mechanisms developed by the IEEE 802.1Qbb work group [3]. In the Priority-based flow control mechanism, traffic requiring low latency is assigned high priority, and the Pause mechanism [15] developed by IEEE 802.3x is applied to traffic within the same priority to guaranty no packets loss. However, the Priority-based Pause mechanism can only solve the transient congestion problem and may cause the saturation tree problem [28] and correspondingly performance degradation facing long-lived congestion. Thus, the end-to-end congestion management mechanism is developed by the IEEE 802.1Qau work group [2] to eliminate the long-lived congestion. It is another indispensable enhancement of Ethernet included in IEEE 802.1 DCB. Moreover, compared to deploying one for each type of traffic in the transport layer, it is more economic to deploy a uniform congestion management scheme in link layer.

The design of end-to-end congestion management mechanisms is challenging due to the special environments and particular requirements in DCE. In general, congestion can be inferred implicitly by packet loss, or detected explicitly by some observable variables, such as round-trip time (RTT) and queue length. However, in DCE, packets cannot be dropped, and it is impossible to estimate RTT due to no ACK. Hence, the queue length is naturally employed to detect congestion in DCE. As a step further, the queue length should be constrained tightly within the buffer size to guarantee low queuing delay and in case the Priority-based Pause mechanism is triggered frequently. However, the buffer of switch is shallow, and thus it is easy to become empty or overflow. The shallow buffer challenges the design of

Manuscript received May 20, 2011; revised June 20, 2012 and June 26, 2013; accepted October 31, 2013; approved by IEEE/ACM TRANSACTIONS ON NETWORKING Editor V. Misra. Date of publication December 11, 2013; date of current version February 12, 2015. This work was supported in part by the National Natural Science Foundation of China (NSFC) under Grant No. 61225011 and the National Basic Research Program of China (973 Program) under Grants No. 2012CB315803 and No. 2010CB328105.

The authors are with the Tsinghua National Laboratory for Information Science and Technology, Department of Computer Science and Technology, Tsinghua University, Beijing 100084, China (e-mail: jiangwc@csnet1.cs.tsinghua.edu.cn; renfy@csnet1.cs.tsinghua.edu.cn; chlin@csnet1.cs.tsinghua.edu.cn).

Color versions of one or more of the figures in this paper are available online at http://ieeexplore.ieee.org.

Digital Object Identifier 10.1109/TNET.2013.2292851

end-to-end congestion management scheme in DCE. In addition, the congestion management scheme should be rate-based instead of window-based since the window size will be limited to only several packets in DCE due to the small RTT. The last but not the least important is that the congestion management scheme should be implemented on hardware to handle traffic in the speed of gigabits per second. Therefore, the congestion control algorithm in DCE must be simple enough.

The IEEE 802.1Qau work group has been working on the end-to-end congestion management scheme of DCE for several years. Up to now, four proposals have been released [2], and Quantized Congestion Notification (QCN) is ratified as the final standard in 2010 [1]. Moreover, QCN has been implemented in devices such as Cisco Nexus 7000 Series [17] and FocalPoint FM6000 [8]. Although QCN has been investigated sufficiently on simulations, implementations, and so on, the theoretical study on QCN is insufficient. The most important reason is that QCN is heuristically designed and involves the property of variable structure. The classic linear analysis method is incapable of handling the segmented nonlinearity of the variable structure system, as we will show in Section II. The developers of QCN show that QCN is stable when the delay is bounded using the frequency-domain analysis [10]. Although they can provide some insight on QCN, the frequency-domain analysis is a classic linear analysis method, and thus they cannot capture the characteristic of the switching process between the rate increase subsystem and rate decrease subsystem in QCN. However, this switching process will imposes significant impacts on the stability, performance, and parameters setting of QCN, as we will show in this paper. Moreover, the frequency-domain analysis method used in [10] cannot explore the dynamic behaviors of QCN.

In this paper, we use the phase plane method, which is suitable for systems of segmented nonlinearity, to analyze the QCN system. We first build a fluid-flow model for the QCN system, and then sketch phase trajectories of the rate increase subsystem and the rate decrease subsystem minutely. Subsequently, taking the switching process between these two subsystems into consideration, we combine these phase trajectories to explore the motion patterns of the phase trajectories describing the global QCN system case by case. As a result, we can provide panorama of the behaviors of the global QCN system. Our analytical results show that the stability of QCN is mainly promised by the sliding mode motion [21]. This is why the queue length always stays close to the target point in the QCN system, as shown in numerous simulations and experiments [14], [30]. However, the range of sliding mode motion region and whether QCN can enter into the sliding mode motion depend on not only the parameters settings but also the network configurations. Moreover, the sufficient conditions for the stability of the QCN system are deduced. They can serve as guidelines toward proper parameters setting. Finally, we implement QCN on the NetFPGA platform [4] and verify the theoretical results through experiments.

The remainder of this paper is arranged as follows. In Section II, the phase plane analysis method is introduced in brief. Subsequently, the core mechanism of QCN is summarized, and the fluid-flow model is constructed. In Section IV, the motion patterns of the phase trajectories describing the QCN system are explored using the phase plane method. Next,

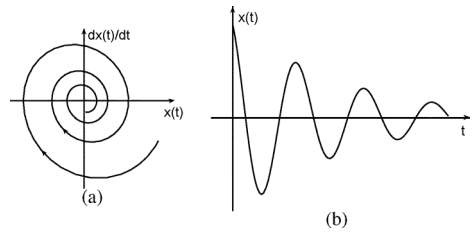

Fig. 1. Example of phase trajectory: (a) phase trajectory and (b) corresponding common trajectory in time domain.

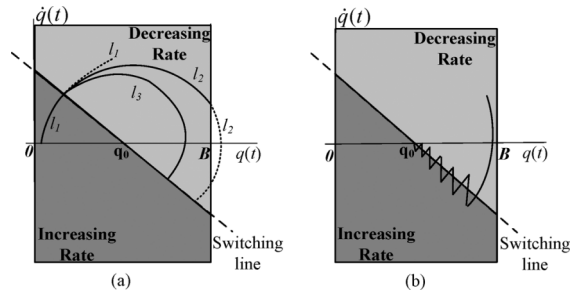

Fig. 2. Example of phase plane analysis on congestion loop. (a) Constraints of buffer size. (b) Sliding mode motion.

the sufficient conditions for the stability of QCN are deduced in Section V. Section VI shows the experimental validation on the NetFPGA platform. Finally, conclusions are drawn in Section VII.

II. Phase Plane Analysis

Phase plane analysis is a graphic method to analyze the behaviors of nonlinear systems, especially systems of segmented nonlinearity. Given an autonomous system described by differential equation $\ddot{x}(t) = f(x(t), \dot{x}(t))$, the phase trajectory of the system can be drawn by connecting points $(x(t), \dot{x}(t))$ along the direction where time t increases. Fig. 1(a) presents a phase trajectory. The corresponding curve of $x(t)$ against time t is displayed in Fig. 1(b). Obviously the evolution of $x(t)$ in time domain can be inferred from the profile of the phase trajectory, and so does the evolution of $\dot{x}(t)$. Thus, the phase trajectory reflects the behaviors of the system with more information than the trajectory on time domain. Moreover, the motion patterns of the phase trajectories reflect the motion patterns of the congestion management system. The existence of various methods, which enable the phase trajectories to be sketched quite accurately, makes the phase plane method superior to finding analytical solution of differential equations, which may not be possible.

Generally, the congestion control scheme in computer networks employs different regulation laws for rate increase and rate decrease, respectively. The switching between rate increase and rate decrease depends on the congestion state. An example is illustrated in Fig. 2(a), where B is the buffer size and $q(t)$ is the queue length. On the phase plane, the queue system starts from the initial point, moves along phase trajectory l_1 in the rate increase region, and then reaches the switching line, which implies the occurrence of certain congestion. Subsequently, the queue system will be controlled by the regulation laws for rate decrease to avoid potential congestion, moving along other phase trajectories, such as l_2 or l_3. In this way, the phase trajectory links the isolated subsystems and presents the switching process graphically. The end point of one subsystem is the initial point of the other subsystem. Thus, the phase plane method is particularly suitable for analyzing a system of segmented

nonlinear characteristics. In fact, the variable structure system is first investigated using the phase plane analysis method by Emelyanov in history [21].

Second, using phase plane method, the physical constraints of buffer size can be included into consideration explicitly. Since the buffer size is limited, if the motion of system follows phase trajectory l_2, the buffer overflows. In this condition, though the system is stable according to the stability criterion in the linear control theory, this motion pattern is not expected in DCE because the overflow of the buffer always indicates dropping packets. Thus, it is crucial to properly fix the buffer size or carefully design the regulation laws to constrain the motions of the system into the shadow area, such as the motion pattern represented by the phase trajectory l_3.

Third, with phase plane method, we can reveal a special phenomenon called sliding mode motion. As shown in Fig. 2(b), when the phase trajectory moves into the rate increase area from the rate decrease area, it may move back to the rate decrease area immediately under the control of the regulation laws for rate increase. Repeating this motion, the trajectory will move toward the equilibrium point along the switching line, independent of the differential equations describing subsystems. As a result, the queue length $q(t)$ chatters around target point q_0 and parameters for the rate increase subsystem and the rate decrease subsystem take no effect to the sliding mode motion excepting the amplitude of the chattering. This special motion pattern also cannot be revealed through the classical analytical approach in linear control theory. However, it may be the dominating behaviors of variable structure systems, such as QCN. Hence, we use the phase plane method to analyze the QCN system in this paper.

III. Modeling QCN

A. Core Mechanism of QCN

The technical goal of the congestion management scheme in DCE is to hold the queue length around the target point tightly such that the buffer is neither overflowed nor underutilized. The overflow of the buffer will trigger the priority-based Pause mechanism, which may degrade the performance of the whole network. Meanwhile, empty buffer means low link utilization. On the contrary, once the queue length is held at the target point, the QCN system is stable, the queuing delay is fixed, the link utilization approaches 100%, and no packet will be dropped. A typical congestion notification scheme developed by the IEEE 802.1Qau work group includes: 1) the congestion detection approach; 2) transferring congestion information from the congestion point to the reaction point; 3) supporting for rate control at the edge of network to shape injecting flows according to the feedback information.

In this section, we will describe the core mechanism of QCN based on the pseudocode ver. 2.3 [27]. More technical details can be found in [2]. As shown in Fig. 3, QCN is composed of two parts:

- *The Congestion Point (CP) or the core switch*: The CP takes charge of detecting congestion, generating feedback messages and sending them to the reaction point.
- *The Reaction Point (RP) or the source*: The RP decreases its sending rate according to the feedback message or increases its sending rate periodically, which is achieved by implementing the rate regulator, such as the leaky bucket algorithm, at the NIC or the edge switch.

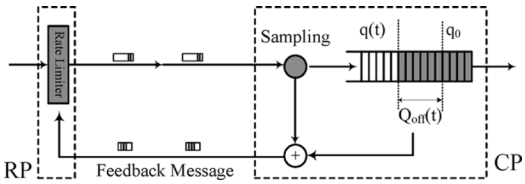

Fig. 3. Framework of QCN: CP is the core switch, and RP can be either NIC or edge switch implementing the rate limiter.

At CP, the congestion is measured by the queue length and its variance. The congestion state information F_b consists of two parts: the current offset of queue length ($Q_{\text{off}} = q(t) - q_0$) and the variance of the queue length in a sampling interval ($\Delta Q = q(t) - q_{\text{old}}$), where q_0 is the target queue length and q_{old} is the queue length at the last time sampling. F_b is given by

$$F_b = -(Q_{\text{off}} + w * \Delta Q) \tag{1}$$

where w is a weight. The switch not only monitors the instantaneous queue length $q(t)$, but also "samples" incoming packets with probability p and generates feedback packets. The sampling probability p is the function of the degree of congestion. The generated feedback packet follows the format of 802.3Tag and is carried to the source address of the sampled packet. In the generated feedback packet, F_b is quantized to 6 bits for the convenience of hardware implementation. Only when $F_b < 0$, i.e., when the buffer is excessive and the queue is building up, feedback packets are generated to ask for reducing the injecting rate. When $F_b > 0$, nothing is signaled. The sending rate is increased actively and rapidly instead.

At RP, let r denote the current sending rate and R denote the sending rate just before the arrival of the latest feedback message. RP starts sending at the rate of the network card and adjusts its sending rate similar to BIC-TCP [29].

Rate Decrease: When a feedback message is received, RP updates R to r and decreases the sending rate r as follows:

$$r \leftarrow r(1 - G_d|F_b|) \tag{2}$$

where G_d is a factor of rate decrease, which is chosen such that $G_d|F_{b\max}| = \frac{1}{2}$, i.e., the sending rate decreases no more than 50% each time.

Rate Increase: Immediately after the rate decrease, RP enters into the state of *Fast Recovery* (FR), increasing the sending rate. FR persists five cycles, and the time length T of each cycle is set to be the time to send 150 kB data by default. At the end of each cycle, R keeps unchanged and r is updated by

$$r \leftarrow \frac{1}{2}(r + R). \tag{3}$$

If no feedback message is received in the period FR, RP enters into the *Active Increase* (AI) state to probe for more available bandwidth. At the state of AI, R and r are updated as follows in each cycle:

$$\begin{cases} R \leftarrow R + R_{\text{AI}} \\ r \leftarrow \frac{1}{2}(r + R) \end{cases} \tag{4}$$

where R_{AI} is the constant unit of rate increase. The time length of each cycle at the state of AI is half of that of FR, i.e., the time to send 75 kB data by default.

Core elements of QCN are the rate adjustment algorithm and the metric to measure congestion. Historically, the AIMD algorithm employed by TCP is inherited as the rate adjustment algorithm in DCE. Subsequently, the rate adjustment algorithm of BIC-TCP is introduced into QCN to be competent for the

high link speed of DCE. The queue length is used to indicate the congestion similar to REM [13] in DCE. With the collaboration of the CP and the RP, the queue length is expected to be held around the target point in the QCN system.

B. Assumption

To model the QCN system, we make four assumptions.

1) Considering the regular and symmetrical network topologies in data centers, such as Fat-Tree [9] and BCube [23], and the special traffic patterns driven by the parallel reads/writes in cluster file systems, such as Lustre [16], the first assumption is that all the sources are homogeneous—namely they have the same characteristics and experience the same round-trip time.
2) The propagation delay in DCE networks is normally within the order of a few microseconds, corresponding to the network radius of several hundred meters. The number of the on-the-fly packets in the link with 10-Gb/s bandwidth and 2-μs propagation delay (which implies that the length of the link is 400 m) is only about 2.[1] Hence, the propagation delay is negligible.
3) Since links are assumed to be of high capacity in DCE networks, the number of bit streams in the links is so large that it appears like continuous flow fluid, the fluid-flow approximation, which is extensively used in network modeling works, such as [25] and [26], is reasonable.
4) In reality, the sampling probability p is designed to be the function of the degree of congestion to reduce the overheads caused by transferring feedback messages. Because large p will add overheads, small p may fail to satisfy the sampling theorem in the condition of heavy congestion. Theoretically, once the sampling theorem is satisfied, the variance of p has little impacts on the behaviors of the QCN system. Therefore, in our analysis, we assume that p is a constant, satisfying the sampling theorem.

C. Fluid-Flow Model of QCN

Given the aforementioned four assumptions, we can model QCN with a set of differential equations. Let $r(t)$ denote the sending rate of each source since sources are homogeneous in DCE networks. The fluid-flow approximation implies that the queue length $q(t)$ and rate $r(t)$ are continuous and differentiable. Considering the queue associated with bottleneck link, we have

$$\frac{dq(t)}{dt} = N\left[r(t) - \frac{C}{N}\right] \tag{5}$$

where N is the number of active flows sharing the bottleneck link and C denotes the capacity of this bottleneck link. The difference of the queue length ΔQ in a sampling interval Δt is

$$\Delta Q = \Delta t \frac{dq(t)}{dt} = \frac{1}{pC}\frac{dq(t)}{dt} \tag{6}$$

where p is the sampling probability. Combining (1), (5), and (6), the feedback variable F_b can be rewritten as

$$F_b = -[q(t) - q_0] - \frac{wN}{pC}\left[r(t) - \frac{C}{N}\right]. \tag{7}$$

[1]On average, we assume that the packet length is 1500 kB. Hence, the number of the on-the-fly packets is $\frac{2\times10^{-6}\times10^{10}}{1500\times8} \approx 1.7$

TABLE I
SUMMARY OF PARAMETERS DEFINITIONS

Parameters	Definitions
C	Link capacity
N	Number of flows sharing bottleneck link
w	Weight of the derivative of queue length
p	Sampling probability
T	Interval of cycle of FR
G_d	Factor for rate decrease
R_{AI}	Unit of rate increase
q_0	Target queue length

Referring to (2), we can obtain the differential equation for rate decrease, i.e., $F_b(t) < 0$

$$\frac{dr(t)}{dt} = G_d F_b(t) r(t). \tag{8}$$

Now, we consider the rate increase subsystem. In reality, the time interval of each cycle of FR and AI can be measured by counters or timers in QCN. We only consider the use of timers for the convenience of modeling. This simplicity does not lose the essence of the FR algorithm, namely the binary search of the proper point for rate recovery. Our model can still reflect the motion patterns of QCN. Let T denote the time interval of each cycle in the state of FR, and the time interval of each cycle in the state of AI is $\frac{T}{2}$. From (3), we can get the differential equation describing the behaviors of QCN in the period of FR

$$\frac{dr(t)}{dt} = \left[\frac{1}{2}(R_0 + r(t)) - r(t)\right] * \frac{1}{T} = \frac{R_0 - r(t)}{2T} \tag{9}$$

where R_0 is the target sending rate of FR, which equals the sending rate just before the latest rate decrease. From (4), we can get the differential equations for the state of AI

$$\frac{dR(t)}{dt} = \frac{R_{\mathrm{AI}}}{\frac{T}{2}} \tag{10}$$

$$\frac{dr(t)}{dt} = \left[\frac{1}{2}(R(t)+r(t)) - r(t)\right] * \frac{2}{T} = \frac{R(t)-r(t)}{T}. \tag{11}$$

So far, the core dynamic behaviors of the QCN system can be described by a set of differential equations, which are of characteristic of segmented nonlinearity. The rate decrease subsystem is described by (5) and (8). The procedure of FR is described by (5) and (9), and the procedure of AI is described by (5), (10), and (11). All the equations aforementioned are related to the queue length $q(t)$ and the sending rate $r(t)$, while $r(t)$ can be expressed by $q(t)$ in (5). Hence, the QCN system can be described by differential equations only associated with $q(t)$, namely the behaviors of the queue system stand for the behaviors of the whole QCN system. Our subsequent analysis will focus on the queue system. Above, only the core mechanism of QCN is modeled. However, the behaviors of the QCN system will also be constrained by the buffer size physically as discussed in Section II. The effects of buffer size can be considered separately in the procedure of phase plane analysis. Next, we will explore the behaviors of the QCN system by analyzing this fluid-flow model using the phase plan method. By the way, to facilitate the search for the definition of parameters, we summarize them in Table I.

IV. BEHAVIORS OF THE QCN SYSTEM

Before analyzing our model quantitatively, we first make the qualitative analysis. More specifically, we analyze the motion

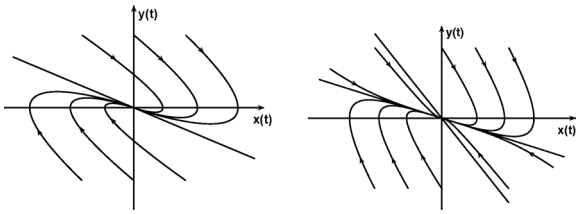

(a) (b)

Fig. 4. Phase trajectories in the rate decrease area when $\zeta \geq 1$. (a) $\zeta > 1$. (b) $\zeta = 1$.

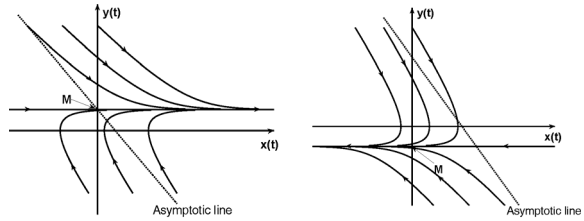

(a) (b)

Fig. 5. Phase trajectories in the procedure of FR. (a) $M > 0$. (b) $M < 0$.

patterns of each subsystem of QCN and then combine these motion patterns to obtain all the possible motion patterns of the global QCN system.

A. Motion Patterns of Subsystems

For the sake of simplicity, we define the variable $k = \frac{w}{pC}$ and make a linear variable substitution

$$\begin{cases} x(t) = q(t) - q_0 \\ y(t) = N * r(t) - C. \end{cases} \tag{12}$$

With this substitution, (7) can be rewritten as

$$F_b = -x(t) - ky(t). \tag{13}$$

Subsequently, we will summarize possible motion patterns when QCN stays in the state of rate decrease, FR and AI, respectively.

1) Rate Decrease: Referring to (5), (8), (12), and (13), we can get the differential equations describing rate decrease subsystem of QCN

$$\begin{cases} \frac{dx(t)}{dt} = y(t) \\ \frac{dy(t)}{dt} = -G_d[x(t) + ky(t)][y(t) + C]. \end{cases} \tag{14}$$

Define functions $g_1(t) = y(t)$ and $g_2(t) = -G_d[x(t) + ky(t)]\,[y(t) + C]$. Since both $g_1(t)$ and $g_2(t)$ are polynomials, for $i = 1, 2$ and any $\vec{z} = (z_1, z_2) = (x(t), y(t))$, there exists L such that $\parallel g_i(t, \vec{z}_1) - g_i(t, \vec{z}_2) \parallel \leq L \parallel \vec{z}_1 - \vec{z}_2 \parallel$, namely the *Lipschitz* condition is satisfied. Hence, the nonlinear differential equations (14) have a solution uniquely determined by the initial value (x_0, y_0) [11]. The origin $(x, y) = (0, 0)$ is obviously a solution of (14), and thus is the singular point. Lyapunov has shown that the stability and the behaviors of nonlinear differential equations in the neighborhood of a singular point can be found from their linearized version about the singular point [18]. The linearized version of (14) at the singular point, i.e., the origin, is

$$\begin{cases} \frac{dx(t)}{dt} = y(t) \\ \frac{dy(t)}{dt} = -G_d C x(t) - \frac{G_d w}{p} y(t). \end{cases} \tag{15}$$

The standard form of this second-order autonomous system is

$$\frac{d^2x(t)}{dt^2} + 2\zeta w_n \frac{dx(t)}{dt} + {w_n}^2 = 0 \tag{16}$$

where $w_n = \sqrt{G_d C}$ and $\zeta = \sqrt{\frac{G_d}{4C}}\frac{w}{p}$. The phase trajectories of a standard formed second-order differential equation have been presented in much literature, such as [12].

- When $\zeta < 1$, i.e., $G_d w^2 < 4Cp^2$, the phase trajectories of differential equation (16) are spirals converging to the origin, and the origin is a stable focus. The motion pattern of the phase trajectories is similar to Fig. 1.
- When $\zeta \geq 1$, i.e., $G_d w^2 \geq 4Cp^2$, the phase trajectories of differential equation (16) are parabolas moving toward the origin, and $(0, 0)$ is a stable node. The motion pattern of the phase trajectories is shown in Fig. 4.

Note that when $\zeta = 1$, the parabolas have only one asymptotic line, while two asymptotic lines for the case $\zeta > 1$.

2) Rate Increase: The procedure of FR is described by (5) and (9). Substituting (12) into (9), we have

$$\frac{dy(t)}{dt} = \frac{NR_0 - C}{2T} - \frac{y(t)}{2T}. \tag{17}$$

Defining $M = NR_0 - C$, we can combine (5) and (17) into a second-order differential equation

$$2T\frac{d^2x(t)}{dt^2} + \frac{dx(t)}{dt} = M. \tag{18}$$

The phase trajectories of this second-order system can be drawn using the isoclinal method [12]. As shown in Fig. 5, all the phase trajectories of differential equation (18), except the line $y(t) = M$, start from infinity with slope $-\frac{1}{2T}$ and approach to the line $y = M$ eventually. The phase trajectories move toward the positive direction of the horizontal axis when $M > 0$, while they move along the opposite direction when $M < 0$. When $M = 0$, the phase trajectories are straight lines with slope $-\frac{1}{2T}$, plus the line $y = 0$, i.e., the abscissa axis.

The procedure of AI is described by (5), (10), and (11). Solving (10), we can get

$$R(t) = \frac{2R_{\mathrm{AI}}}{T}t + R_0. \tag{19}$$

Combining (11), (12), (19), and (5), we can obtain the differential equations for the AI procedure

$$\frac{dy(t)}{dt} = \frac{2NR_{\mathrm{AI}}}{T^2}t + \frac{NR_0 - C}{T} - \frac{y(t)}{T}. \tag{20}$$

We can further combine (5) and (20) into a second-order differential equation

$$T\frac{d^2x(t)}{dt^2} + \frac{dx(t)}{dt} = \frac{2NR_{\mathrm{AI}}}{T}t + M. \tag{21}$$

The differential equation above is similar to (18), and so are the corresponding phase trajectories. However, in the procedure of AI, the slope of phase trajectories starting from infinity are $-\frac{1}{T}$, and finally all the phase trajectories will move along the lines with slope $\frac{2NR_{\mathrm{AI}}}{T^2}$ instead of the line $y = M$. When $M < 0$, the phase trajectories defined by differential equation (21) turn to the negative direction of horizontal axis for a while, but its final direction is decided by slope $\frac{2NR_{\mathrm{AI}}}{T^2}$ instead of the sign of M. The phase trajectories of differential equation (21) corresponding to the sign of M are shown in Fig. 6(a) and (b), respectively.

3) Switching Process: The main association of subsystems is the initial states. More specifically, as shown in Fig. 5, the

motion pattern of the rate increase subsystem depends on its initial state, namely the sign of $M = NR_0 - C$, instead of the parameters setting. Let r_0 denote the initial sending rate of FR, and R_0 denote the target sending rate of FR. The sending rate changes from R_0 to r_0 when the QCN system switches from the rate decrease subsystem into the rate increase subsystem. Since the sending rate is decreased by no more than 50% each time, we have

$$Nr_0 - C < M = NR_0 - C \leq 2Nr_0 - C. \tag{22}$$

M also indicates the degree of congestion: $M > 0$ means the congestion is heavy since the rate is decreased by a large amount, $M < 0$ means the congestion is slight on the contrary. The motion pattern of the global QCN system changes itself depending on the degree of congestion. Moreover, whether QCN enters into the procedure of AI also depends on the degree of congestion, namely whether the sending rate can be recovered in the procedure of FR. Subsequently, combining possible phase trajectories in each subsystem, we will explore possible motion patterns of the global QCN system case by case.

B. Motion Patterns of the Global QCN System

Generally speaking, the initial state of the QCN system is $(-q_0, y(0))$, where $y(0)$ is a very large value since sources start at the rate of the network card. Therefore, the initial state of the QCN system is in the rate decrease area. The queue length will increase and exceed the target point q_0 quickly after the initial regulation process, i.e., it will reach the point $(0, \nu)$ promptly, where $\nu > 0$. We start our analysis of the QCN system from point $(0, \nu)$. Starting from point $(0, \nu)$, the phase trajectory of the QCN system is decided by (16) first. In the rate decrease area, if $\zeta < 1$, the phase trajectory is spiral. When $\zeta \geq 1$, the phase trajectory is parabola. The value of ζ is decided by the parameters setting.

1) Case 1 (Parabola or $\zeta \geq 1$): Since the phase trajectories of the rate decrease subsystem differ from each other when $\zeta = 1$ and $\zeta > 1$, as shown in Fig. 4, the global QCN system has two motion patterns in this case.

• If the switching line Γ $(F_b(t) = 0)$ is below the asymptotic line of the parabola in the fourth quadrant, the phase trajectory of QCN will approach to the origin directly without passing Γ. The corresponding motion pattern is shown in Fig. 4.

• If the switching line Γ is above the asymptotic line of the parabola in the fourth quadrant, the phase trajectory of QCN will reach Γ in the fourth quadrant starting from $(0, \nu)$ in the rate decrease area. Fig. 7 illustrates this phenomenon. Phase trajectories l_1 and l_3 are similar to that in Fig. 4, describing the motion patterns of the rate decrease subsystem. The phase trajectory of the global QCN system will move along the solid part of l_1 first, and then pass through Γ. The following phase trajectory is l_2, which denotes the procedure of rate increase. Finally, the phase trajectory of the global QCN system will move back to the rate decrease area, following the solid part of l_3 after passing Γ again, and then converge to the origin directly.

In summary, when $\zeta \geq 1$, the phase trajectory of QCN will move to the origin after passing through Γ zero or twice.

2) Case 2 (Spiral or $\zeta < 1$): Starting from the point $(0, \nu)$ in the rate decrease area, the phase trajectory of QCN will reach the switching line Γ in the fourth quadrant after a period of time. Assume that the ith time the phase trajectory of QCN reaches the switching line at point (x_0^i, y_0^i) via the rate decrease area and

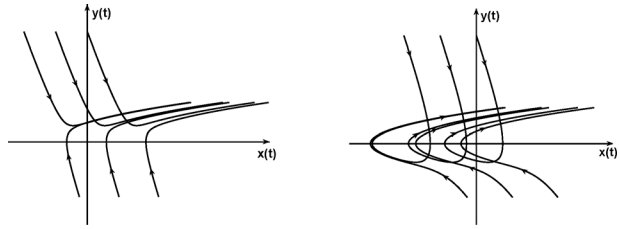

(a) (b)

Fig. 6. Phase trajectories in the procedure of AI. (a) $M \geq 0$. (b) $M < 0$.

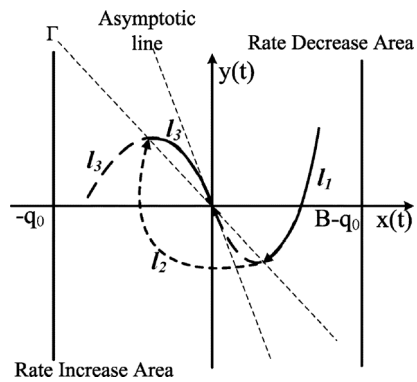

Fig. 7. Phase trajectory of the global QCN system when $\zeta \geq 1$.

R_i is the corresponding target sending rate for the following fast recovery. In this way, (22) can be rewritten as

$$-\frac{x_0^i}{k} < M_i = NR_i - C < C - \frac{2x_0^i}{k}. \tag{23}$$

Point (x_0^1, y_0^1) exists when QCN starts from $(0, \nu)$. Furthermore, $x_0^i > 0$ in the fourth quadrant. After passing point (x_0^i, y_0^i), the phase trajectory of QCN has several possible motion patterns according to Fig. 5, depending on both the parameters setting and the system states. Subsequently, we will show these possible motion patterns case by case. For the convenience of discussion, let (x_1^i, y_1^i) denote the ith time the phase trajectory of QCN reaches the switching line via the rate increase area.

Sliding Mode Motion Pattern: Passing point (x_1^i, y_1^i), the phase trajectory of QCN may move back to the rate decrease area immediately after it enters into the rate increase area, as shown in Fig. 8. Intuitively, the curve ① and curve ② in Fig. 8 are corresponding to the cases $M_i \geq 0$ and $M_i < 0$, respectively. When the phase trajectory of the global QCN system is composed by the spiral in the rate decrease area and curve ① or curve ② in the rate increase area, the QCN system enters into the sliding mode motion as we have discussed in Section II. In the sliding mode motion, the phase trajectory of the global QCN system approaches to the origin along the switching line Γ by switching between the rate decrease area and the rate increase area frequently. The following proposition shows the exact cases in which the sliding mode motion occurs.

Proposition 1: The sliding mode motion pattern occurs in any of the following cases:

① $2T \leq k$ and $M_i \geq 0$;

② $2T < k$, $M_i < 0$ and $x_0^i \geq \frac{k^2 M_i}{2T-k}$;

③ $2T > k$, $M_i \geq 0$ and $x_0^i \leq \frac{k^2 M_i}{2T-k}$.

Proof: The necessary and sufficient condition for the occurrence of the sliding mode motion is $\lim_{F_b(t)\to 0} \dot{F}_b(t) \leq 0$ [12].

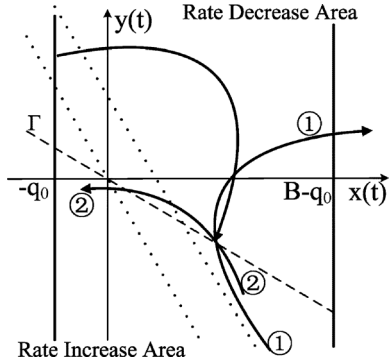

Fig. 8. Possible phase trajectory of the global QCN system when $2T \leq k$. Curves ① and ② are taken from Fig. 5(a) and (b), respectively.

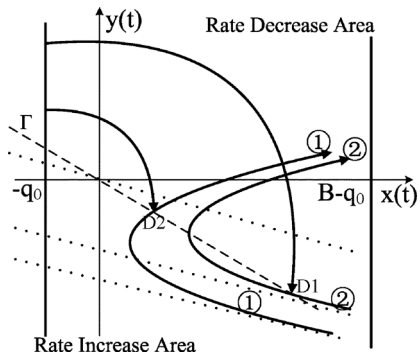

Fig. 9. Possible phase trajectory of the global QCN system when $2T > k$. Curve ① and ② are taken from Fig. 5(a).

- Referring to (16) and (13), inequality $\lim_{F_b(t)\to 0^-} \dot{F}_b(t) \geq 0$ is equivalent to inequality $\frac{x_0^i}{k} \geq 0$. In the fourth quadrant, inequality $\frac{x_0^i}{k} \geq 0$ holds. Thus, the switching line is reachable from the rate decrease area.
- Furthermore, referring to (18) and (13), inequality $\lim_{F_b(t)\to 0^+} \dot{F}_b(t) \leq 0$ is equivalent to

$$(2T-k)x_0^i \leq k^2 M_i. \tag{24}$$

Obviously, inequality (24) holds when any of the above three conditions is satisfied. ■

Except for Fig. 8, which is the sketch map of Cases ① and ② of Proposition 1, we represent the Case ③ of Proposition 1 by the phase trajectory ① in Fig. 9.

Normal Motion Pattern: If QCN does not enter into the sliding mode motion, the phase trajectory of QCN will be dominated by (18) in the procedure of FR after passing point (x_0^i, y_0^i) in the switching line Γ. Then, it either moves back to the rate decrease area in $5T$, but not immediately, or enters into the procedure of AI after $5T$. In both cases, the phase trajectory of QCN finally moves back to the rate decrease area, according to Figs. 5 and 6. Therefore, (x_1^i, y_1^i) exists. Since the phase trajectory of QCN is spiral in the rate decrease area, (x_0^{i+1}, y_0^{i+1}) must exist when (x_1^i, y_1^i) exists. Passing point (x_0^i, y_0^i) from the rate decrease area, several motion patterns may occur according to Figs. 5 and 6.

Curve ② in Fig. 9 shows a possible motion pattern that the phase trajectory of QCN moves back to the rate decrease area in $5T$. Passing point (x_0^i, y_0^i), the phase trajectory of QCN moves along curve ②, then reaches the switching line Γ at point (x_1^i, y_1^i), and finally moves back to the switching line Γ at point (x_0^{i+1}, y_0^{i+1}) along the spirals.

Proposition 2: Passing point (x_0^i, y_0^i), the phase trajectory of QCN can move back to the rate decrease area in $5T$ in the following case.

④ $2T > k$, $M_i \geq 0$ and $\frac{k^2 M_i}{2T-k} < x_0^i \leq \frac{k^2 M_i}{2T-k}[1 + \frac{3T+2Te^{-2.5}}{k(1-e^{-2.5})}] \approx \frac{k^2 M_i}{2T-k}(1+\frac{3T}{k})$

Proof: Since $\frac{k^2 M_i}{2T-k} < x_0^i$, the QCN system would never enter into the sliding mode motion referring to Proposition 1.

In the procedure of FR, the solution of (18) is

$$\begin{cases} x(t) = 2T\left(M_i + \frac{x_0^i}{k}\right)e^{-\frac{t}{2T}} + M_i t + x_0^i \\ \qquad\quad -2T\left(M_i + \frac{x_0^i}{k}\right) \\ y(t) = M_i - \left(M_i + \frac{x_0^i}{k}\right)e^{-\frac{t}{2T}}. \end{cases} \tag{25}$$

Define function

$$\begin{aligned} f(t) &= x(t) + ky(t) \\ &= (2T-k)\left(M_i + \frac{x_0^i}{k}\right)\left(e^{-\frac{t}{2T}} - 1\right) + M_i t. \end{aligned} \tag{26}$$

Then, the derivative of function $f(t)$ is

$$\frac{df(t)}{dt} = M_i - \frac{1}{2T}(2T-k)\left(M_i + \frac{x_0^i}{k}\right)e^{-\frac{t}{2T}}. \tag{27}$$

Since $2T > k$ and $M_i \geq 0$, function $\frac{df(t)}{dt}$ is strictly monotone increasing. Let $t = 0$, there is

$$\begin{aligned} \frac{df(0)}{dt} &= M_i - \frac{1}{2T}(2T-k)\left(M_i + \frac{x_0^i}{k}\right) \\ &= \frac{k^2 M_i + (k-2T)x_0}{2T} \\ &< \frac{k^2 M_i - k^2 M_i}{2T} \\ &= 0. \end{aligned} \tag{28}$$

The bound holds because $\frac{k^2 M_i}{2T-k} < x_0^i$ and $2T > k$. Hence, function $\frac{df(t)}{dt}$ increases from negative to positive with the increase of time t. Because $f(0) = 0$ and $\lim_{t\to+\infty} \frac{df(t)}{dt} = M_i \geq 0$, function $f(t)$ decreases to be negative at first and then increases to be positive with the increase of time t. Since function $f(t)$ is continuous, $f(t) = 0$ has a unique solution t_4 except $t = 0$. Furthermore, $f(t) > 0$ for any $t \in (t_4, +\infty)$.

On the other hand, referring to (25), there is

$$\begin{aligned} f(5T) &= 5TM_i - (1-e^{-2.5})\left(2TM_i + \frac{2Tx_0^i}{k} - kM_i - x_0^i\right) \\ &= \left[\frac{5T}{k} - \frac{2T}{k}(1-e^{-2.5}) + 1 - e^{-2.5}\right]kM_i \\ &\quad - (1-e^{-2.5})\left(\frac{2T}{k} - 1\right)x_0^i \\ &\geq \left[\frac{5T}{k} - \frac{2T}{k}(1-e^{-2.5}) + 1 - e^{-2.5}\right]kM_i \\ &\quad - (1-e^{-2.5})\left[1 + \frac{3T+2Te^{-2.5}}{k(1-e^{-2.5})}\right]kM_i \\ &= 0. \end{aligned} \tag{29}$$

The bound holds because $x_0^i \leq \frac{k^2 M_i}{2T-k}[1 + \frac{3T+2Te^{-2.5}}{k(1-e^{-2.5})}]$. Hence, $t_4 \leq 5T$. It means Case ④ is sufficient for the phase trajectory of QCN moving back to the rate decrease area in $5T$. ■

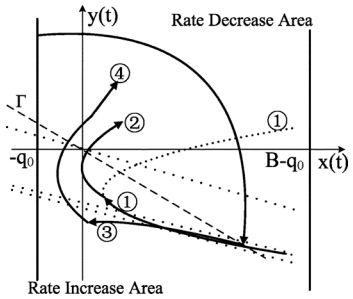

Fig. 10. Possible phase trajectory of the global QCN system with $2T > k$. Curve ①, ②, ③, and ④ are taken from Figs. 5(a), 6(a), 5(b) and 6(b), respectively.

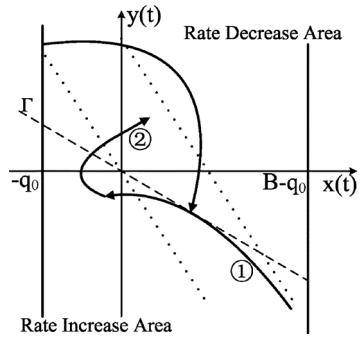

Fig. 11. Possible phase trajectory of the global QCN system with $2T \leq k$. Curve ①and ②are taken from Figs. 5(b) and 6(b), respectively.

In the rest of the cases, the phase trajectory of QCN cannot move back to the rate decrease area in $5T$, and the QCN system will enter into the procedure of AI after $5T$. In the procedure of AI, the phase trajectory of QCN is controlled by differential equation (21), and the corresponding phase trajectories are shown in Fig. 6. Subsequently, according to Fig. 6, the phase trajectory of QCN will pass through the switching line at point (x_1^i, y_1^i) and then follow the spiral until reaching the switching line at point (x_0^{i+1}, y_0^{i+1}) from the rate decrease area.

Proposition 3: Passing point (x_0^i, y_0^i), the phase trajectory of QCN can not move back to the rate decrease area in $5T$ in the following cases:

⑤ $2T < k$, $M_i < 0$ and $x_0^i < \frac{k^2 M_i}{2T-k}$

⑥ $2T \geq k$ and $M_i < 0$;

⑦ $2T > k$, $M_i \geq 0$ and $x_0^i > \frac{k^2 M_i}{2T-k}[1 + \frac{3T+2Te^{-2.5}}{k(1-e^{-2.5})}]$.

Proof: Similar to the proof of Proposition 2, we will show that $f(5T) < 0$ in all of the three cases here.

- When Case ⑤ holds, referring to (22) and (27), we can know that function $\frac{df(t)}{dt}$ decreases with the increase of time t and accordingly $\frac{df(t)}{dt} < \frac{df(0)}{dt}$. Similar to (28), we can also deduce that $\frac{df(0)}{dt} < 0$. In total, there is $f(5T) < f(0) = 0$.
- When Case ⑥ holds, referring to (22) and (27), we have $\frac{df(t)}{dt} < 0$. Hence, $f(5T) < f(0) = 0$.
- When Case ⑦ holds, $f(5T) < 0$ according to (29).

In all the three cases, since $f(5T) < 0$, the phase trajectory of QCN cannot return back to the rate decrease area in $5T$. ■

The combination of phase trajectories ① and ② in Fig. 10 represents Case ⑦ of Proposition 3, the combination of phase trajectories ③ and ④ in Fig. 10 represents Case ⑥ of Proposition 3, and the combination of phase trajectories ① and ② in Fig. 11 represents Case ⑤ of Proposition 3.

C. Discussion

In (23) and Cases ②, ③, ④, ⑤, and ⑦, variables x_0^i and M_i are bounded by each other. Consequently, some of the corresponding motion patterns may be impossible to occur. For example, we can deduce that $M_i < 2Nr_0 - C = C - 2y_0^i = C - \frac{2x_0^i}{k}$ from (23). Hence, when $M_i \geq 0$, there is $x_0^i < \frac{kC}{2}$. If $\frac{kC}{2} < \frac{k^2 M_i}{2T-k}$, Cases ④ and ⑦ would never occur. On the contrary, all the possible motion patterns of the global QCN system have been explored since Cases ①–⑦ make up a complete set.

In sum, starting from the initial states, the phase trajectory of QCN has several possible motion patterns due to the system states and the parameters setting. We have studied all of them case by case. When $\zeta \geq 1$, i.e., $G_d w^2 \geq 4p^2 C$, the phase trajectory of QCN converges to the origin without switching or switching twice. When any of Cases ①–③ is satisfied, the sliding mode motion pattern occurs. In these cases, the phase trajectory of QCN will move toward the origin directly along the switching line. When any of the rest of the cases is satisfied, the phase trajectory of QCN will first reach the switching line at point (x_0^1, y_0^1) from the rate decrease area. Then, starting from point (x_0^i, y_0^i) in the switching line, the phase trajectory of QCN moves to point (x_0^{i+1}, y_0^{i+1}) in the switching line from the rate increase area with different motion patterns. The value of i keeps increasing.

V. Stability Analysis of QCN

A. Preliminary

Based on the above qualitative analysis, we do quantitative analysis to provide sufficient conditions for the stability of QCN. More specifically, we explore sufficient conditions such that $x_0^{i+1} < x_0^i$ for each possible motion pattern of the global QCN system. If $x_0^{i+1} < x_0^i$ for each motion pattern, the value of x_0^i decreases with the increase of i until $x_0^i = 0$, namely QCN enters into the stable state gradually. In contrast to the motion patterns being separated by conditions associated with M_i and x_0^i, the sufficient conditions provided here should be independent of M_i and x_0^i since these two parameters are associated with the system state.

Moreover, as we have shown in Fig. 2(a), the phase trajectory of QCN may be disturbed by the limited buffer size. The overflow of buffer cannot be tolerated in the QCN system since it will result in pausing links, in which condition the network is stalled and latency becomes unacceptable large. Hence, the maximum buffer size should be estimated quantitatively. Considering the special requirements of DCE, we introduce the conception of strong stability for the QCN system.

Definition 1: If $\forall t$, $q(t) < B$, where B is the buffer size and $q(t)$ is the queue length in the buffer, the QCN system is strongly stable.

B. Stability Analysis

Now we will analyze the strong stability of the QCN system case by case. When the QCN system switches from one subspace to another, we recalculate the time, i.e., the endpoint of the behaviors in one subspace is the beginning of the behaviors in the next subspace.

1) Case 1 ($\zeta \geq 1$): In this case, the phase trajectory of QCN approaches to the origin without switching or switching twice. Namely, $x_0^1 = 0$ or $x_0^2 = 0$. However, referring to the strong sta-

bility of the QCN system, we still need to consider the physical constraints of buffer size B. The solutions $\lambda_{1,2}$ of the characteristic equation of (16) are

$$\lambda_{1,2} = -\zeta w_n \pm w_d \tag{30}$$

where $w_d = \sqrt{\zeta^2 - 1} w_n$.

- If $\zeta = 1$, the two real eigenvalues of differential (16) are identical, i.e., $\lambda_{1,2} = \lambda = -\zeta w_n$. Thus, the solution of differential equation (16) is

$$\begin{cases} x(t) = (A_3 + A_4 t)e^{\lambda t} \\ y(t) = (A_4 + A_4 \lambda t)e^{\lambda t} \end{cases} \tag{31}$$

where A_3 and A_4 are constant decided by the initial value. With initial value $(x(0), y(0)) = (0, \nu)$, we have $A_3 = 0$ and $A_4 = \nu$. Since $y(t) = \dot{x}(t)$, we can get the maximum of $x(t)$ by solving t from equation $y(t) = 0$. The solution is $t = -\frac{1}{\lambda}$, and thus the maximum of $x(t)$ is

$$x_{\max 1} = -\frac{\nu}{\lambda} e^{-1} = \frac{\nu}{\zeta w_n} e^{-1} < \frac{\nu}{\zeta w_n} = \frac{2p\nu}{G_d w} < \frac{\nu}{w_n}. \tag{32}$$

- If $\zeta > 1$, the two real eigenvalues of differential equation (16) are different from each other. Thus, the solution of differential equation (16) is

$$\begin{cases} x(t) = A_1 e^{\lambda_1 t} + A_2 e^{\lambda_2 t} \\ y(t) = A_1 \lambda_1 e^{\lambda_1 t} + A_2 \lambda_2 e^{\lambda_2 t} \end{cases} \tag{33}$$

where A_1 and A_2 are constants decided by the initial values. Rearranging (33), we have

$$[y(t) - \lambda_1 x(t)]^{\lambda_1} = C_0 [y(t) - \lambda_2 x(t)]^{\lambda_2} \tag{34}$$

where $C_0 = \frac{[(\lambda_2 - \lambda_1)A_2]^{\lambda_1}}{[(\lambda_1 - \lambda_2)A_1]^{\lambda_2}}$. Equation (34) confirms that the phase trajectories of the rate decrease subsystem are parabolas when $\zeta > 1$. Substituting the initial value $(0, \nu)$ into (34), we can get $C_0 = \nu^{\lambda_1 - \lambda_2}$. When $y(t) = 0$ in (34), $x(t)$ reaches its maximum, which can be computed as follows:

$$\begin{aligned} x_{\max 2} &= \nu \left[\frac{(-\lambda_2)^{\lambda_2}}{(-\lambda_1)^{\lambda_1}} \right]^{\frac{1}{\lambda_1 - \lambda_2}} \\ &= \nu \left(\frac{\lambda_2}{\lambda_1} \right)^{\frac{\lambda_2}{\lambda_1 - \lambda_2}} \frac{1}{-\lambda_1} \\ &= \frac{\nu}{\zeta w_n + w_d} \left(\frac{\zeta w_n - w_d}{\zeta w_n + w_d} \right)^{\frac{\zeta w_n - w_d}{2 w_d}}. \end{aligned} \tag{35}$$

Since $\zeta > 1$, $w_n, w_d > 0$, and $\zeta w_n > \sqrt{\zeta^2 - 1} w_n = w_d$, there is

$$x_{\max 2} < \frac{\nu}{\zeta w_n + w_d} < \frac{\nu}{\zeta w_n} = \frac{2p\nu}{G_d w} < \frac{\nu}{w_n}. \tag{36}$$

In sum, we have the following lemma.

Lemma 1: If $\zeta \geq 1$ and $\frac{2p\nu}{G_d w} \leq B - q_0$, the QCN system is strongly stable.

2) Case 2 ($\zeta < 1$): In this case, the phase trajectories of rate decrease subsystem are spirals. The solutions $\lambda_{1,2}$ of the characteristic equation of differential equation (16) are complex conjugate in this case

$$\lambda_{1,2} = -\zeta w_n \pm j w_d \tag{37}$$

where $w_d = \sqrt{1 - \zeta^2} w_n$. The solution of (16) is

$$\begin{cases} x(t) = A e^{-\zeta w_n t} \cos(w_d t + \varphi) \\ y(t) = -A\zeta w_n e^{-\zeta w_n t} \cos(w_d t + \varphi) \\ \qquad -A w_d e^{-\zeta w_n t} \sin(w_d t + \varphi) \end{cases} \tag{38}$$

where A and φ are coefficients decided by the initial values.

$$\begin{cases} A = \frac{1}{w_d} \sqrt{[\zeta w_n x(0) + y(0)]^2 + [w_d x(0)]^2} \\ \varphi = -\arctan \frac{y(0) + \zeta w_n x(0)}{w_d x(0)}. \end{cases} \tag{39}$$

Assume the spiral starting from point $(-q_0, \frac{q_0}{k})$ reaches the switching line Γ at point $(x_0^{\max}, y_0^{\max})$. Due to the physical constraints of the buffer size B, there is $x_0^i \leq x_0^{\max}$ for any $i \geq 1$. Substituting the initial value $(-q_0, \frac{q_0}{k})$ into (39), we can get the explicit expression of A and φ with parameters of QCN. Then, from (38) and $x(t) + ky(t) = 0$, we can work out the time t_0 that the phase trajectory of QCN takes to move from point $(-q_0, \frac{q_0}{k})$ to point $(x_0^{\max}, y_0^{\max})$ via the rate decrease area. The solution is $t_0 = \frac{\pi}{w_d}$, and thus

$$x_0^{\max} = x(t_0) = q_0 e^{-\frac{\zeta w_n \pi}{w_d}} = q_0 e^{-\frac{\zeta \pi}{\sqrt{1 - \zeta^2}}}. \tag{40}$$

Similarly, we can know that

$$x_0^{i+1} = |x_1^i| \, e^{-\frac{\zeta \pi}{\sqrt{1 - \zeta^2}}}. \tag{41}$$

When QCN starts from the initial value $(0, \nu)$, the phase trajectory of QCN will reach the switching line Γ at point (x_0^1, y_0^1) in the fourth quadrant. Since $y_0^1 < 0 < \nu$, there exists t_1 such that $y(t_1) = 0$. Since $y(t) = \dot{x}(t)$ and $y(t_1) = 0$, $x_{\max 3} = x(t_1)$ is the maximum of $x(t)$. The value of $x_{\max 3}$ can be computed similar to (40)

$$x_{\max 3} = \frac{\nu}{\sqrt{(\zeta w_n)^2 + {w_d}^2}} e^{-\frac{\zeta w_n}{w_d}(\frac{\pi}{2} - \arctan \frac{\zeta w_n}{w_d})} < \frac{\nu}{w_n} \tag{42}$$

Crossing the switching line Γ at point (x_0^i, y_0^i), the phase trajectory of QCN will be dominated by differential equation (18), and then the sending rate will be increased. At this point, several motion patterns may occur as we have shown in Section VI. Subsequently, we will analyze them one by one.

In *Cases* ①–③, the phase trajectory of QCN follows the sliding mode motion pattern and converges to the origin along the switching line directly. Thus, there is $0 < x_0^{i+1} \leq x_0^i$ in all of these three cases.

In *Case* ④, inequalities $2T > k$, $M_i \geq 0$ and $\frac{k^2 M_i}{2T - k} < x_0^i \leq \frac{k^2 M_i}{2T - k}(1 + \frac{3T + 2Te^{-2.5}}{k(1 - e^{-2.5})}) \approx \frac{k^2 M_i}{2T - k}(1 + \frac{3T}{k})$ hold. The phase trajectory of QCN moves back to the rate decrease area in $5T$. Assume the phase trajectory reaches the switching line at point (x_1^i, y_1^i) at time t_4. Referring to (26), t_4 is the solution of $f(t_4) = 0$, i.e.,

$$\left(M_i + \frac{x_0^i}{k} \right) e^{-\frac{t_4}{2T}} = M_i + \frac{x_0^i}{k} - \frac{M_i t_4}{2T - k} > 0. \tag{43}$$

Substituting (43) into (25), we have

$$\begin{aligned} x_1^i &= x(t_4) \\ &= -k y(t_4) \\ &= k \left(M_i + \frac{x_0^i}{k} \right) e^{-\frac{t_4}{2T}} - k M_i \\ &= x_0^i - \frac{k M_i t_4}{2T - k} < x_0^i \end{aligned} \tag{44}$$

and

$$-x_1^i = k M_i - k \left(M_i + \frac{x_0^i}{k} \right) e^{-\frac{t_4}{2T}} < \frac{k M_i (2T - k)}{2T - k}. \tag{45}$$

Therefore, when $T < k$, inequality $|x_1^i| < x_0^i$ holds, and thus $x_0^{i+1} < x_0^i e^{-\frac{\zeta \pi}{\sqrt{1 - \zeta^2}}}$ referring to (41).

In *Cases* ⑤–⑦, the phase trajectory of QCN enters into the procedure of AI after $5T$, and then moves back to the rate decrease area by passing the switching line at point (x_1^i, y_1^i). Referring to (25), the initial value of the AI procedure is

$$\begin{cases} x(5T) = 5TM_i + x_0^i + 2T\left(M_i + \frac{x_0^i}{k}\right)(e^{-2.5} - 1) \\ y(5T) = M_i - \left(M_i + \frac{x_0^i}{k}\right)e^{-2.5}. \end{cases} \tag{46}$$

The solution of the differential equation (21), which constrains the phase trajectories of the AI procedure, is

$$\begin{cases} \bar{x}(t) = T[M_i - y(5T) - 2NR_{\rm AI}]e^{-\frac{t}{T}} \\ \quad +\frac{NR_{\rm AI}}{T}t^2 + [M_i - 2NR_{\rm AI}]t + x(5T) \\ \quad -T[M_i - y(5T) - 2NR_{\rm AI}] \\ \bar{y}(t) = [y(5T) + 2NR_{\rm AI} - M_i]e^{-\frac{t}{T}} + \frac{2NR_{\rm AI}}{T}t \\ \quad +[M_i - 2NR_{\rm AI}]. \end{cases} \tag{47}$$

From (46) and (23), we can deduce that

$$M_i - y(5T) = \left(M_i + \frac{x_0^i}{k}\right)e^{-2.5} > 0. \tag{48}$$

With this result, the derivative of $\bar{y}(t)$ satisfies

$$\frac{d\bar{y}(t)}{dt} = \frac{2NR_{\rm AI}}{T}\left(1 - e^{-\frac{t}{T}}\right) + \frac{M_i - y(5T)}{T}e^{-\frac{t}{T}} > 0. \tag{49}$$

Thus, function $\bar{y}(t)$ increases with the increase of the time t. Let t_5 denote the interval of the AI procedure and define function $f_1(t) \triangleq \bar{x}(t) + k\bar{y}(t)$. There are $f_1(t_5) = 0$ and

$$x_1^i = -k\bar{y}(t_5) < -k\bar{y}(0) = -ky(5T) < -kM_i < x_0^i. \tag{50}$$

On the other hand, $f_1(t_5) = 0$ can be rewritten as

$$\begin{aligned} &\frac{NR_{\rm AI}}{T}t_5^2 + M_i t_5 + x(5T) + Ty(5T) = (T-k) \\ &\times\left[M_i - \left(M_i + \frac{x_0^i}{k}\right)e^{-2.5-\frac{t_5}{T}} + 2NR_{\rm AI}\left(e^{-\frac{t_5}{T}} - 1 + \frac{t_5}{T}\right)\right]. \end{aligned} \tag{51}$$

Substituting (51) and (46) into (47), we have

$$\begin{aligned} -x_1^i &= k\bar{y}(t_5) \\ &= k\left[M_i - \left(M_i + \frac{x_0^i}{k}\right)e^{-2.5-\frac{t_5}{T}}\right. \\ &\quad \left. +2NR_{\rm AI}\left(e^{-\frac{t_5}{T}} - 1 + \frac{t_5}{T}\right)\right] \\ &= \frac{k}{T-k}\left[\frac{NR_{\rm AI}}{T}t_5^2 + M_i t_5 + Ty(5T) + x(5T)\right] \\ &= \frac{k}{k-T}\left[-\frac{NR_{\rm AI}}{T}\left(t_5 + \frac{TM_i}{2NR_{\rm AI}}\right)^2\right. \\ &\quad \left. +\frac{TM_i{}^2}{4NR_{\rm AI}} - Ty(5T) - x(5T)\right]. \end{aligned} \tag{52}$$

Consequently, we can deduce as follows:

$$\begin{aligned} &-x_1^i < x_0^i \\ &\Leftrightarrow k\left[\frac{NR_{\rm AI}}{T}t_5^2 + M_i t_5 + Ty(5T) + x(5T)\right] > (T-k)x_0^i \\ &\Leftrightarrow \frac{kNR_{\rm AI}}{T}t_5^2 + kM_i t_5 + 4TkM_i + 2kx_0^i - 3Tx_0^i \\ &\quad + T\left(kM_i + x_0^i\right)e^{-2.5} > 0 \\ &\Leftrightarrow t_5 > \frac{-TkM_i + \sqrt{\Omega}}{2kNR_{\rm AI}} > \frac{-TM_i}{NR_{\rm AI}} \end{aligned} \tag{53}$$

where

$$\begin{aligned} \Omega = T^2k^2M_i^2 + 4TkNR_{\rm AI}&\left[3Tx_0^i - 2kx_0^i\right. \\ &\left. -4TkM_i - T\left(kM_i + x_0^i\right)e^{-2.5}\right]. \end{aligned} \tag{54}$$

Once $\Omega < 0$, inequality (53) holds. The derivation of function $f_1(t)$ is

$$\begin{aligned} \frac{df_1(t)}{dt} = \frac{2NR_{\rm AI}}{T}t + M_i + \frac{k-T}{T}&\left[2NR_{\rm AI}\left(1 - e^{-\frac{t}{T}}\right)\right. \\ &\left. +\left(M_i + \frac{x_0^i}{k}\right)e^{-2.5-\frac{t}{T}}\right]. \end{aligned} \tag{55}$$

Therefore, when $t \geq \frac{-TM_i}{2NR_{\rm AI}}$, there is $\frac{df_1(t)}{dt} > 0$, and thus function $f_1(t)$ is monotone increasing function. Accordingly, once the inequality $f_1(\frac{-TkM_i+\sqrt{\Omega}}{2kNR_{\rm AI}}) < f_1(t_5) = 0$ holds, there is $t_5 > \frac{-TkM_i+\sqrt{\Omega}}{2kNR_{\rm AI}}$, and thus inequality (53) holds. Referring to (51), we have

$$\begin{aligned} f_1\left(\frac{-TkM_i + \sqrt{\Omega}}{2kNR_{\rm AI}}\right) = (k-T)&\left[2NR_{\rm AI}\left(e^{\frac{TkM_i - \sqrt{\Omega}}{2TkNR_{\rm AI}}} - 1\right)\right. \\ &\left. +\frac{\sqrt{\Omega}}{Tk} - \frac{x_0^i}{k} - \left(M_i + \frac{x_0^i}{k}\right)e^{-2.5+\frac{TkM_i-\sqrt{\Omega}}{2TkNR_{\rm AI}}}\right]. \end{aligned} \tag{56}$$

Subsequently, we will provide sufficient conditions for either $\Omega < 0$ or $f_1(\frac{-TkM_i+\sqrt{\Omega}}{2kNR_{\rm AI}}) < 0$.

In *Case* ⑤, inequalities $2T < k$, $M_i < 0$, and $x_0^i < \frac{k^2M_i}{2T-k}$ hold.

- We first consider the subcase that $k \geq 3.5T$. Referring to (54), we have

$$\begin{aligned} \Omega &< T^2k^2M_i^2 + 4TkNR_{\rm AI}\left[(3T - 7T)x_0^i - 4TkM_i\right. \\ &\quad \left. -T\left(kM_i + x_0^i\right)e^{-2.5}\right] \\ &< T^2k^2M_i^2 + 16T^2kNR_{\rm AI}\left(-kM - x_0^i\right) \\ &< T^2k^2M_i^2 \\ &< T^2{x_0^i}^2. \end{aligned} \tag{57}$$

  Substituting this result into (56), we have

$$f_1\left(\frac{-TkM_i + \sqrt{\Omega}}{2kNR_{\rm AI}}\right) < (k-T)\left(\frac{\sqrt{\Omega}}{Tk} - \frac{x_0^i}{k}\right) < 0. \tag{58}$$

  Therefore, when $k \geq 3.5T$, $M_i < 0$, and $x_0^i < \frac{k^2M_i}{2T-k}$, inequality $-x_1^i < x_0^i$ holds. As a step further, referring to inequality (50) and (41), there is $|x_1^i| < x_0^i$ in this subcase, and thus $x_0^{i+1} < x_0^i e^{-\frac{\zeta\pi}{\sqrt{1-\zeta^2}}}$.

Summarizing Cases ①, ②, and this subcase of Case ⑤ and referring to (42), we have the following lemma.

Lemma 2: The QCN system is strongly stable when $\frac{\nu}{w_n} < B - q_0$ and $k \geq 3.5T$.

- Secondly, we will consider the subcase that $2.5T < k < 3.5T$. Define $\theta = -\frac{NR_{\rm AI}}{M_i}$. In (54), since $M > -\frac{x_0^i}{k}$, there is

$$\begin{aligned} \Omega &< T^2k^2M_i^2 + 4TkNR_{\rm AI}[(3T - 2k)x_0^i - 4TkM_i] \\ &= T^2k^2M_i^2 + 4\theta TkM_i[4TkM_i - (2k - 3T)kM_i] \\ &= T^2k^2M_i^2(4\phi\theta + 1) \end{aligned} \tag{59}$$

where $\phi = \frac{7T-2k}{T}$. Define function

$$f_2(t) = (k-T)\left[2NR_{\mathrm{AI}}\left(e^{\frac{TkM_i-t}{2TkNR_{\mathrm{AI}}}}-1\right)+\frac{t}{Tk} -\frac{x_0^i}{k}-\left(M_i+\frac{x_0^i}{k}\right)e^{-2.5+\frac{TkM_i-t}{2TkNR_{\mathrm{AI}}}}\right]. \quad (60)$$

We can know that $f_2(\sqrt{\Omega}) = f_1(\frac{-TkM_i+\sqrt{\Omega}}{2kNR_{\mathrm{AI}}})$ and $f_2(t)$ is monotone increasing function since

$$\frac{df_2(t)}{dt} = \frac{k-T}{Tk}\left[1-e^{\frac{TkM_i-t}{2TkNR_{\mathrm{AI}}}}\left(1-\frac{M_i+\frac{x_0^i}{k}}{2NR_{\mathrm{AI}}}e^{-2.5}\right)\right] > 0. \quad (61)$$

Hence

$$\begin{aligned} &f_1\left(\frac{-TkM_i+\sqrt{\Omega}}{2kNR_{\mathrm{AI}}}\right)\\ &= f_2(\sqrt{\Omega})\\ &< f_2(-TkM_i\sqrt{4\phi\theta+1})\\ &= (k-T)\left[-2\theta M_i\left(e^{-\frac{1+\sqrt{4\phi\theta+1}}{2\theta}}-1\right)-\frac{x_0^i}{k}\right.\\ &\qquad \left.-M_i\sqrt{4\phi\theta+1}-\left(M_i+\frac{x_0^i}{k}\right)e^{-2.5-\frac{1+\sqrt{4\phi\theta+1}}{2\theta}}\right]. \end{aligned} \quad (62)$$

If $\sqrt{4\phi\theta+1}+2\theta(e^{-\frac{1+\sqrt{4\phi\theta+1}}{2\theta}}-1) < 0$, then $f_1(\frac{-TkM_i+\sqrt{\Omega}}{2kNR_{\mathrm{AI}}}) < 0$. Or else, since $-M_i < \frac{x_0^i}{k}$, there is

$$f_1\left(\frac{-TkM_i+\sqrt{\Omega}}{2kNR_{\mathrm{AI}}}\right) < \frac{(k-T)x_0^i}{k}\left[2\theta\left(e^{-\frac{1+\sqrt{4\phi\theta+1}}{2\theta}}-1\right) +\sqrt{4\phi\theta+1}-1\right]. \quad (63)$$

Define function $f_3(\theta) = 2\theta(e^{-\frac{1+\sqrt{4\phi\theta+1}}{2\theta}}-1)+\sqrt{4\phi\theta+1}-1$ and let $s=\sqrt{4\phi\theta+1}$, we have

$$f_3(s) = \frac{s-1}{2\phi}\left[(s+1)e^{-\frac{2\phi}{s-1}}-s+2\phi-1\right]. \quad (64)$$

Define function $f_4(s) = (s+1)e^{-\frac{2\phi}{s-1}}-s+2\phi-1$. The derivative of function $f_4(s)$ is

$$\begin{cases} \frac{df_4(s)}{ds} = e^{-\frac{2\phi}{s-1}}\left[\frac{4\phi}{(s-1)^2}+\frac{2\phi}{s-1}+1\right]-1\\ \frac{d^2f_4(s)}{ds^2} = e^{-\frac{2\phi}{s-1}}\frac{1}{(s-1)^3}\left[\frac{8\phi^2}{s-1}+4\phi^2-8\phi\right]. \end{cases} \quad (65)$$

Since $2.5T < k < 3.5T$, there is $0 < \phi < 2$. When $s \geq \frac{2+\phi}{2-\phi}$, i.e., $\theta \geq \frac{2T^2}{(2k-5T)^2}$, we have $\frac{d^2f_4(s)}{ds^2} \leq 0$, and thus $\frac{df_4(s)}{ds}$ is monotone decreasing function. Assume s^* satisfies equation $\frac{df_4(s^*)}{ds}=0$. When $s > s^*$, $\frac{df_4(s)}{ds} < 0$, and thus $f_4(s)$ is monotone decreasing function in $[s^*,+\infty]$. Conversely, when $s < s^*$, $\frac{df_4(s)}{ds} > 0$, and thus $f_4(s)$ is monotone increasing function in $[0,s^*]$. Consequently, we have $f_4(s) \leq f_4(s^*)$. On the other side, when $\frac{df_4(s^*)}{ds}=0$, there is

$$e^{-\frac{2\phi}{s^*-1}} = \frac{(s^*-1)^2}{(s^*-1)^2+2\phi(s^*-1)+4\phi} \quad (66)$$

and thus

$$\begin{aligned} f_4(s^*) &= \frac{(s^*-1)^2(s^*+1)}{(s^*-1)^2+2\phi(s^*-1)+4\phi}-s+2\phi-1\\ &= \frac{(4\phi^2-8\phi)s^*+4\phi^2}{(s^*-1)^2+2\phi(s^*-1)+4\phi}\\ &\leq \frac{4\phi(\phi-2)\frac{2+\phi}{2-\phi}+4\phi^2}{(s^*-1)^2+2\phi(s^*-1)+\phi^2+4\phi-\phi^2}\\ &= \frac{-8\phi}{(s^*-1+\phi)^2+\phi(4-\phi)}\\ &< 0. \end{aligned} \quad (67)$$

With this result and referring to (63), we have

$$\begin{aligned} f_1\left(\frac{-TkM_i+\sqrt{\Omega}}{2kNR_{\mathrm{AI}}}\right) &< \frac{(k-T)x_0^i}{k}f_3(\theta)\\ &= \frac{(k-T)x_0^i}{k}f_3(s)\\ &= \frac{(k-T)x_0^i}{k}\frac{s-1}{2\phi}f_4(s)\\ &\leq \frac{(k-T)x_0^i}{k}\frac{s-1}{2\phi}f_4(s^*) < 0. \end{aligned} \quad (68)$$

In total, when $2.5T < k < 3.5T$, $M_i < 0$, $x_0^i < \frac{k^2M_i}{2T-k}$, and $NR_{\mathrm{AI}} = -\theta M_i \geq \frac{-2T^2M_i}{(2k-5T)^2}$, inequality $-x_1^i < x_0^i$ holds. As a step further, referring to inequality (50) and (41), there is $|x_1^i| < x_0^i$ in this subcase, and thus $x_0^{i+1} < x_0^i e^{-\frac{\zeta\pi}{\sqrt{1-\zeta^2}}}$.

Summarizing Cases ①, ②, and this part of Case ⑤ and referring to (40) and (42), we have the following lemma.

Lemma 3: The QCN system is strongly stable when $\frac{\nu}{w_n} < B-q_0$, $2.5T < k < 3.5T$ and $NR_{\mathrm{AI}} \geq \frac{2T^2x_0^{\max}}{(2k-5T)^2k} \geq \frac{2T^2x_0^i}{(2k-5T)^2k} > \frac{-2T^2M_i}{(2k-5T)^2}$.

- Thirdly, we will consider the subcase that $k \leq 2.5T$. In this subcase, we have $2 \leq \phi \leq 3$. Hence, referring to (65), there is $\frac{d^2f_4(s)}{ds^2} > 0$, and thus $\frac{df_4(s)}{ds}$ is a monotone increasing function. Assume s^* satisfies $\frac{df_4(s^*)}{ds}=0$. When $s > s^*$, $\frac{df_4(s)}{ds} > 0$, and thus $f_4(s)$ is a monotone increasing function in $[s^*,+\infty]$. Conversely, when $s < s^*$, $\frac{df_4(s)}{ds} < 0$, and thus $f_4(s)$ is a monotone decreasing function in $[0,s^*]$. Consequently, we have $f_4(s) \geq f_4(s^*)$. Since $\frac{df_4(s^*)}{ds}=0$, (66) holds, and thus

$$f_4(s^*) = \frac{(4\phi^2-8\phi)s^*+4\phi^2}{(s^*-1)^2+2\phi(s^*-1)+4\phi} > 0. \quad (69)$$

The bound holds because $\phi \geq 2$. On the other side, when $M_i \to -\frac{x_0^i}{k}$, referring to (54), we have

$$\Omega \to T^2{x_0^i}^2+4T(7T-2k)\theta{x_0^i}^2 = \sqrt{4\phi\theta+1}Tx_0^i. \quad (70)$$

Substituting (69) and (70) into (56), we can know that when $M_i \to -\frac{x_0^i}{k}$, there is

$$\begin{aligned} f_1\left(\frac{-TkM_i+\sqrt{\Omega}}{2kNR_{\rm AI}}\right) &\to (k-T)\left[\frac{\sqrt{4\phi\theta+1}Tx_0^i}{Tk}-\frac{x_0^i}{k}\right. \\ &\left.+2NR_{\rm AI}\left(e^{\frac{TkM_i-\sqrt{4\phi\theta+1}Tx_0^i}{2TkNR_{\rm AI}}}-1\right)\right] \\ &= \frac{(k-T)x_0^i}{k}f_3(\theta) = \frac{(k-T)x_0^i}{k}f_3(s) \\ &= \frac{(k-T)x_0^i}{k}\frac{s-1}{2\phi}f_4(s) \geq \frac{(k-T)x_0^i}{k}\frac{s-1}{2\phi}f_4(s^*) \\ &> 0. \end{aligned} \tag{71}$$

Therefore, when $k \leq 2.5T$, we cannot provide sufficient condition for either $\Omega < 0$ or $f_1(\frac{-TkM_i+\sqrt{\Omega}}{2kNR_{\rm AI}}) < 0$.

In *Case* ⑥, inequalities $2T \geq k$ and $M_i < 0$ hold. Thus, there is $\phi = \frac{7T-2k}{T} \geq 3$, and M_i can be close to $-\frac{x_0^i}{k}$. Consequently, (71) holds, and thus we cannot provide sufficient condition for either $\Omega < 0$ or $f_1(\frac{-TkM_i+\sqrt{\Omega}}{2kNR_{\rm AI}}) < 0$.

In *Case* ⑦, inequalities $2T > k$, $M_i \geq 0$, and $x_0^i > \frac{k^2M_i}{2T-k}[1+\frac{3T+2Te^{-2.5}}{k(1-e^{-2.5})}] \approx \frac{k^2M_i}{2T-k}(1+\frac{3T}{k})$ hold. When $T < k$, there is

$$\begin{aligned} -x_1^i &= \frac{k}{k-T}\left[-\frac{NR_{\rm AI}}{T}t_5^2 - M_it_5 - Ty(5T) - x(5T)\right] \\ &< \frac{k}{k-T}[-Ty(5T) - x(5T)] \\ &= \frac{k}{k-T}\left[\frac{2T-k}{k}x_0^i - 4TM_i - T\left(M_i+\frac{x_0^i}{k}\right)e^{-2.5}\right] \\ &< \frac{k}{k-T}\left[\frac{2T-k}{k}x_0^i - \frac{4T(2T-k)}{k(k+3T)}x_0^i\right] \\ &= \frac{2T-k}{k+3T}x_0^i \\ &< x_0^i. \end{aligned} \tag{72}$$

The first bound holds because $M_i \geq 0$ and $\frac{NR_{\rm AI}}{T} > 0$. The second bound holds because $x_0^i \geq \frac{k^2M_i}{2T-k}[1+\frac{3T+2Te^{-2.5}}{k(1-e^{-2.5})}] \approx \frac{k^2M_i}{2T-k}(1+\frac{3T}{k})$. Therefore, from (50) and (72), there is $|x_1^i| < x_0^i$ when $T < k$. As a step further, referring to (41), there is $x_0^{i+1} < x_0^i e^{-\frac{\zeta\pi}{\sqrt{1-\zeta^2}}}$.

C. Discussion

1) Stability: We can summarize all the three lemmas into the following theorem.

Theorem 1: If $\frac{\nu}{\sqrt{G_dC}} \leq B - q_0$, and any of the following conditions is satisfied, the QCN system is strongly stable.

1) $\zeta \geq 1$, i.e., $\sqrt{\frac{G_d}{4C}}\frac{w}{p} \geq 1$;
2) $\zeta < 1$ and $k \geq 3.5T$, i.e., $\sqrt{\frac{G_d}{4C}}\frac{w}{p} < 1$ and $\frac{w}{pC} \geq 3.5T$;
3) $3.5T \geq k \geq 2.5T$ and $NR_{\rm AI} \geq \frac{2T^2x_0^{\max}}{(2k-5T)^2k}$, i.e., $3.5T \geq \frac{w}{pC} \geq 2.5T$ and $NR_{\rm AI} \geq \frac{2T^2q_0}{(2k-5T)^2k}e^{-\frac{\zeta\pi}{\sqrt{1-\zeta^2}}} = \frac{2T^2C^3p^3q_0}{w(2w-5TCp)^2}e^{-\frac{\sqrt{G_d}w\pi}{\sqrt{4Cp^2-G_dw^2}}}$.

In reality, $\zeta = \sqrt{\frac{G_d}{4C}}\frac{w}{p} \ll 1$. Hence, it is conditions 2) and 3) that mainly take effect in reality in Theorem 1. Consequently, the comparison between T and $k = \frac{w}{Cp}$ is crucial. However, the value of k is decided by not only parameters w and p but also parameter C. Given a fixed parameters setting, the QCN system may not be able to reach the stable state when the available bandwidth C changes. When the Ethernet speed increases to 100 Gb/s, the range of the variation of C becomes large. In this situation, it will be hard to set parameters T for QCN.

Moreover, conditions 2) and 3) are obtained from Cases ①, ②, and part of Case ⑤. Because M_i, which represents the target sending rate of the procedure of FR, would rarely become negative in reality, the state of QCN mainly stays in Case ①. It means that QCN approaches to the stable state mainly through the sliding mode motion. That is why the queue length always stays close to the target point as shown in simulations and experiments [14], [30].

In addition, summarizing cases ①, ③, ④, and ⑦, we know that inequality $x_0^{i+1} < x_0^i e^{-\frac{\zeta\pi}{\sqrt{1-\zeta^2}}}$ holds when $T \leq k$ and $M_i \geq 0$. Since this conclusion is associated with M_i, it cannot be taken as the sufficient condition for the stability of the QCN system. However, since M_i would rarely become negative in reality, we can usually have the following conclusion, which is stronger than Theorem 1.

Conclusion: If $\frac{\nu}{\sqrt{G_dC}} \leq B - q_0$, $\zeta < 1$ and $k \geq T$, the QCN system is strongly stable.

When any of the three sufficient conditions in Theorem 1 is satisfied, there are $x_0^{i+1} < x_0^i e^{-\frac{\zeta\pi}{\sqrt{1-\zeta^2}}}$. Hence, we can know not only that QCN is strongly stable, but also that with the increase of i, the convergence speed of x_0^i is exponential.

2) Buffer Size: The Priority-based Pause mechanism is developed to avoid dropping packets. When it is triggered, the latency will become unexpectedly large, even if the long-term tree saturation can be eliminated by QCN. Thus, the Priority-based Pause mechanism works as the last insurance of no packets loss. It is still crucial to set buffer size properly for QCN to avoid triggering the Priority-based Pause mechanism frequently.

Assume that $C = 10$ Gb/s and the propagation delay is 10 μs in DCE. According to the classical rule-of-thumb for buffer dimensioning, the buffer size is suggested to be 100 kb. Theorem 1 shows the largest queue length is $q_0 + N\sqrt{\frac{C}{G_d}}$ when the QCN system starts from $(0, \nu)$ and is stable. Assume $q_0 = 33$ kb, $G_d = \frac{1}{128}$, and $N = 50$, as recommended in [14]. Theorem 1 tells that the strongly stable QCN system requires 56 Mb buffer size when QCN starts at the rate of NIC, i.e., $\nu = N * C$, whereas about 1.2 Mb buffer size when the initial sending rate of each source is $\frac{C}{N}$, i.e., $\nu = C$. Therefore, it is reasonable to set the initial sending rate to a smaller value than the rate of NIC, and set the buffer size larger than the bandwidth delay product in QCN.

VI. Experiments

The NetFPGA [4] platform is a programmable hardware platform for fast prototyping. A NetFPGA card consists of a Xilinx Virtex-II Pro FPGA, four 1-Gb/s Ethernet ports, and 4 MB SRAM. The advantages of using NetFPGA are that a lot of reference designs can be extended, the ability of handing data in speed of Gb/s, and memory-mapped I/O registers accessed by host PC, which can help to solve the intractable debug problem in hardware design. The disadvantage is the limited number of ports in each NetFPGA card. To verify our theoretical analysis, we implement the core mechanism of QCN on the NetFPGA platform.

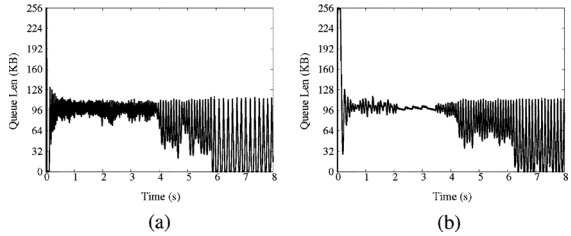

Fig. 12. Evolution of the queue length at the bottleneck link with different parameters. (a) Parameter T is changed. (b) Parameter p is changed.

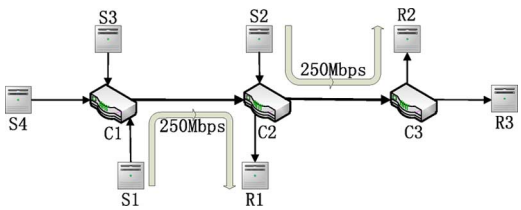

Fig. 13. Parking lot topology.

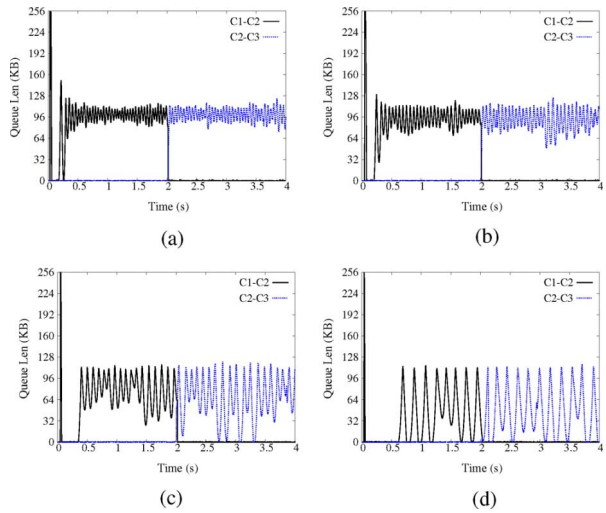

Fig. 14. Evolution of the queue length at the bottleneck link on the parking lot topology. (a) $T_b = 50$ kB. (b) $T_b = 75$ kB. (c) $T_b = 150$ kB. (d) $T_b = 300$ kB.

Unless declared explicitly, all the experiments use the following default parameters and configurations. The link capacity is 1 Gb/s. The link lengths are within 10 m. The output buffer size of switch is 256 kB. The default parameters for the CP of QCN are $w = 2$, $p = 0.01$, and $q_0 = 96$ kB. F_b is quantized to 6 bits in the feedback packets. The default parameters for the RP of QCN are $G_d = \frac{1}{128}$, $R_{\text{AI}} = 1$ Mb/s, and T is the time to send $T_b = 150$ kB data. Under the default parameters setting, there are $\zeta = \sqrt{\frac{G_d}{4C}}\frac{w}{p} \ll 1$.

The experiments are first conducted using a three-sources dumbbell topology. We let sources start long-lived flows at the speed of 1 Gb/s, and then change parameter T every 2 s. From beginning to the end, there are $T_b = 50$ kB, $T_b = 75$ kB, $T_b = 150$ kB, $T_b = 300$ kB, and accordingly $3.5T < k$, $2.5T < k < 3.5T$, $T < k < 2T$, $k < T$, respectively. The evolution of the queue length at the bottleneck link is shown in Fig. 12(a). Corresponding to our conclusion, when $k > T$ in the first 6 s, the buffer almost never becomes empty or full, and the QCN system is stable. More specifically, the queue length only chatters around the target point in the first 4 s. This is consistent with what we have discussed around Theorem 1. Namely, in reality, conditions 2) and 3) of Theorem 1 mainly take effect, and QCN approaches to the stable state mainly through the sliding mode motion. On the contrary, when $k < T$ in the last 2 s, the buffer becomes empty frequently, and the QCN system becomes unstable.

Similar experimental results on parameter p are shown in Fig. 12(b). Parameter p is changed every 2 s, and the values of p are 0.0025, 0.005, 0.01, and 0.02, respectively. Correspondingly, there are $3.5T < k$, $2.5T < k < 3.5T$, $T < k < 2T$, and $k < T$, respectively. Obviously, the evolution of the queue length in Fig. 12(b) has the same trends as in Fig. 12(a). Therefore, these result verify Theorem 1 as well.

Secondly, we verify our theoretical results on the parking lot topology. As shown in Fig. 13, C1, C2, and C3 are CPs. S1 and S2 start background flows of fixed size 250 Mb/s destined to R1 and R2 in $[0s, 2s]$ and $[2s, 4s]$, respectively. S3 and S4 are RPs who start long-lived flows destined to R3. Obviously, the bottleneck link is C1-C2 in $[0s, 2s]$ and changes to be C2-C3 in $[2s, 4s]$. Experiments are repeated with different parameter T, and the corresponding results are shown in Fig. 14. The evolution of the queue length in Fig. 14 has the same trends as in Fig. 12(a). Therefore, in the same way, these results also agree with Theorem 1.

VII. Conclusion

Recently, QCN has been ratified to be the standard for the end-to-end congestion management mechanism over Ethernet, which is a step further in enhancing Ethernet to be the unified switch fabric of DCNs. Because QCN is heuristically designed and involves the property of variable structure, the theoretical insights on QCN are insufficient. Using the phase plane method, which is suitable for systems of variable structure, we analyze the QCN system in this paper. We present the panorama of the behaviors of the QCN system and deduce several sufficient conditions for the strongly stable QCN system. These sufficient conditions can directly serve as the guidelines toward proper parameters settings of QCN. Theoretical analysis shows that the stability of QCN system is mainly ensured by the sliding mode motion, which is also the reason for the chattering of the queue length in reality. However, the range of sliding mode motion region and whether QCN can enter into the sliding mode motion depend on not only the parameters settings but also the network configurations. Thus, the performance of QCN depends on not only the parameters settings but also the network configurations. Finally, experiments on the NetFPGA platform verify the theoretical results.

Acknowledgment

The authors gratefully acknowledge the anonymous reviewers for their constructive comments.

References

[1] "IEEE 802.1: Data Center Bridging Task Group," 2013 [Online]. Available: http://www.ieee802.org/1/pages/dcbridges.html
[2] "IEEE 802.1Qau: End-to-end congestion management," Working Draft, 2011 [Online]. Available: http://www.ieee802.org/1/pages/802.1au.html
[3] "IEEE 802.1Qbb: Priority-based flow control," Working Draft, 2011 [Online]. Available: http://www.ieee802.org/1/pages/802.1bb.html

[4] "NetFPGA project," [Online]. Available: http://netfpga.org/
[5] Cisco, San Jose, CA, USA, "Unified computing," [Online]. Available: http://www.cisco.com/en/US/netsol/ns944/index.html#~in_depth
[6] Cisco, San Jose, CA, USA, "Unified fabric: Cisco's innovation for data center networks," White Paper, 2008 [Online]. Available: http://www.cisco.com/en/US/solutions/collateral/ns340/ns517/ns224/ns783/white_paper_c11-462422.pdf
[7] "100 Gigabit Ethernet," 2010 [Online]. Available: http://en.wikipedia.org/wiki/100_Gigabit_Ethernet
[8] "Fulcrum announces 1 billion packet per second 10G/40G Ethernet switch chips for efficient scaling of virtualized data center networks," Nov. 2010 [Online]. Available: http://www.businesswire.com/news/home/20101101006001/en/Fulcrum-Announces-1-Billion-Packet-10G40G-Ethernet
[9] M. AI-Fares, A. Loukissas, and A. Vahdat, "A scalable, commodity data center network architecture," in *Proc. ACM SIGCOMM*, Aug. 2008, pp. 63–74.
[10] M. Alizadeh, B. Atikoglu, A. Kabbani, A. Lakshmikantha, R. Pan, B. Prabhakar, and M. Seaman, "Data center transport mechanisms: Congestion control theory and IEEE standardization," in *Proc. 46th Annu. Allerton Conf.*, Sep. 2008, pp. 1270–1277.
[11] V. Arnol'd, *Ordinary Differential Equations*. New York, NY, USA: Springer-Verlag, 1992.
[12] D. P. Atherton, *Nonlinear Control Engineering*. New York, NY, USA: Van Nostrand Reinhold, 1982.
[13] S. Athuraliya, V. H. Li, S. H. Low, and Q. Yin, "REM: Active queue management," *IEEE Netw.*, vol. 15, no. 3, pp. 48–53, Jan. 2001.
[14] B. Atikoglu, A. Kabbani, R. Pan, B. Prabhakar, and M. Seaman, "The origin, evolution and current status of QCN," 2007 [Online]. Available: http://www.ieee802.org/1/files/public/docs2008/au_prabhakar_qcn_evolution_summary.pdf
[15] H. Barrass, "Definition for new PAUSE function rev 1.0," 2007 [Online]. Available: http://www.ieee802.org/1/files/public/docs2007/new-cm-barrass-pause-proposal.pdf
[16] P. J. Braam, "File systems for cluster from a protocol perspective," in *Proc. 2nd Extreme Linux Topics Workshop*, Monterey, CA, USA, 1999 [Online]. Available: http://www.cs.cmu.edu/~coda/docdir/extremelinux99.pdf
[17] B. Chia, "DC technology update," 2010 [Online]. Available: http://www.cisco.com/web/SG/learning/dc_partner/files/Nexus_Update.pdf
[18] E. Coddington and N. Levionson, *Theory of Ordinary Differential Equations*. New York, NY, USA: McGraw-Hill, 1975.
[19] D. Cohen, T. Talpey, A. Kanevsky, U. Cummings, M. Krause, R. Recio, D. Crupnicoff, L. Dickman, and P. Grun, "Remote direct memory access over the converged enhanced ethernet fabric: Evaluating the options," in *Proc. High Perform. Interconnects*, 2009, pp. 123–130.
[20] C. DeSanti and J. Jiang, "FCoE in perspective," in *Proc. Int. Conf. Adv. Infocomm Technol.*, 2008, pp. 1–8.
[21] S. V. Emel'yanov, *Automatic Control Systems of Variable Structure*. Moscow, Russia: Nauka, 1967.
[22] B. Goglin, "Design and Implementation of Open-MX: High-performance message passing over generic ethernet hardware," in *Proc. IEEE IPDPS*, 2008, pp. 1–7.
[23] C. Guo, G. Lu, D. Li, H. Wu, X. Zhang, Y. Shi, C. Tian, Y. Zhang, and S. Lu, "BCube: A high performance, server-centric network architecture for modular data centers," in *Proc. ACM SIGCOMM*, Aug. 2009, pp. 63–74.
[24] M. Gusat, C. Minkenberg, and G. J. Paljak, "Flow and congestion control for datacenter networks," 2009 [Online]. Available: http://domino.research.ibm.com/library/cyberdig.nsf/papers/C6313FBBF3770E8D8525768F003629B2/$File/rz3742.pdf
[25] Y. Lu, R. Pan, B. Prabhakar, D. Bergamasco, V. Alaria, and A. Baldini, "Congestion control in networks with no congestion drops," in *Proc. 44th Allerton Annu. Conf. Commun., Control, Comput.*, Sep. 2007 [Online]. Available: http://www.stanford.edu/~balaji/papers/au-Lu-et-al-BCN-study.pdf
[26] V. Misra, W. Gong, and D. Towsley, "Fluid-based analysis of a network of AQM routers supporting TCP flows with an application to RED," in *Proc. ACM SIGCOMM*, Aug. 2000, pp. 151–160.
[27] R. Pan, "QCN pseudo code version 2.3," 2009 [Online]. Available: http://www.ieee802.org/1/files/public/docs2009/au-rong-qcn-serial-hai-v23.pdf
[28] G. Pfister and V. Norton, "Hot spot contention and combining in multistage interconnection networks," *IEEE Trans. Comput.*, vol. C-34, no. 10, pp. 933–938, Oct. 1985.
[29] L. Xu, K. Harfoush, and I. Rhee, "Binary increase congestion control (BIC) for fast long-distance networks," in *Proc. IEEE INFOCOM*, Mar. 2004, pp. 2514–2524.
[30] M. Yasuda, N. Kobayashi, K. Ichino, A. Kader, Kabanni, and B. Prabhakar, "10G QCN implementation on hardware," Nov. 2009 [Online]. Available: http://ieee802.org/1/files/public/docs2009/au-yasuda-10G-QCN-Implementation-1109.pdf

Wanchun Jiang received the B.E. degree in computer science and technology from Tsinghua University, Beijing, China, in 2009, and is currently pursuing the Ph.D. degrees in computer science and technology at Tsinghua University under the supervision of Prof. Fengyuan Ren and Prof. Chuang Lin.

His research interests include congestion control, Ethernet, data center networks, and the application of control theory in computer networks.

Fengyuan Ren (M'04) received the B.A. and M.Sc. degrees in automatic control and Ph.D. degree in computer science from Northwestern Polytechnical University, Xi'an, China, in 1993, 1996, and 1999, respectively.

He is a Professor with the Department of Computer Science and Technology, Tsinghua University, Beijing, China. From 2000 to 2001, he worked with the Electronic Engineering Department, Tsinghua University, as a Post-Doctoral Researcher. In 2002, he moved to the Computer Science and Technology Department, Tsinghua University. He (co)authored more than 80 international journal and conference papers. His research interests include network traffic management, control in/over computer networks, wireless networks, and wireless sensor networks.

Prof. Ren has served as a technical program committee member and local arrangement chair for various IEEE and ACM international conferences.

Chuang Lin (M'03–SM'04) received the Ph.D. degree in computer science from Tsinghua University, Beijing, China, in 1994.

He is a Professor with the Department of Computer Science and Technology, Tsinghua University. He is an Honorary Visiting Professor with the University of Bradford, Bradford, U.K. His current research interests include computer networks, performance evaluation, network security analysis, and Petri net theory and its applications. He has published more than 300 papers in research journals and IEEE conference proceedings in these areas and has published four books.

Prof. Lin is the Chinese Delegate in TC6 of IFIP. He served as the Technical Program Vice Chair of the 10th IEEE Workshop on Future Trends of Distributed Computing Systems (FTDCS 2004); the General Chair of the ACM SIGCOMM Asia Workshop 2005 and the 2010 IEEE International Workshop on Quality of Service (IWQoS 2010). He is an Associate Editor of the IEEE TRANSACTIONS ON VEHICULAR TECHNOLOGY and an Area Editor of *Computer Networks* and the *Journal of Parallel and Distributed Computing*.